Laboratory Dynamo Experiments

Gautier Verhille, Nicolas Plihon, Mickaël Bourgoin, Philippe Odier, Jean-François Pinton

Laboratory dynamo experiments

Gautier Verhille, Nicolas Plihon, Mickael Bourgoin,
Philippe Odier, and Jean-François Pinton
Laboratoire de Physique de l'École Normale Supérieure de Lyon,
CNRS & Université de Lyon, F-69364 Lyon, France

(Dated: March 21, 2009)

I. INTRODUCTION

Although dynamo research is essentially motivated by observations from planetary and stellar dynamos, the conditions that prevail in such natural objects cannot be reproduced in the laboratory. Experiments and numerics can only be run in quite different parameter regimes, but they both provide useful insights into the features of natural dynamos. Experiments cannot be rotated as fast as real systems do, convective motion cannot be as strong, etc, but they run with real fluids and probe quantities that cannot be accessed from remote observations of natural dynamos. Numerical experiments record the complete dynamical fields in space and time (but at quite removed parameter values) while laboratory experiments but probe a limited part of the velocity and magnetic fields, $\mathbf{u}, \mathbf{B}$. The two approaches are complementary and have been associated in most recent works. Numerical development are reported in several contributions to this volume. We focus here on the specific issues involved in the actual implementation of an experimental dynamo and recall the findings of recent studies. The reader is also referred to reviews that have recently been published [1–4].

In order for a dynamo to be self-sustained, the production of induced currents by fluid motions must overcome the resistive Joule dissipation. This condition sets an instability threshold, requiring that the magnetic Reynolds number of the flow ($R_M = UL/\lambda$) exceeds a critical value R_M^c – U and L are characteristic velocity and length and λ is the magnetic diffusivity. An energy-based criterion for generation inside a sphere gives a lower bound $R_M^c > \pi^2$ [5]. For more complex geometries, and taking into account real flow structure there is no general expression for R_M^c – on the contrary, theorems prevent the action of dynamo action for too simple geometries [5]. Assuming R_M^c values of the order of 10 to 100 (a value often quoted for the Earth), and given the fact that all liquid metals have magnetic Prandtl numbers (ratio of kinetic to magnetic diffusivities) of the order of $P_M \sim 10^{-6}$, one realizes that dynamo flows are associated with huge kinetic Reynolds number values $R_V = R_M/P_M$, typically exceeding 10^6. Such high R_V values are associated with fully developed turbulence, an observation that raises several central issues for dynamo experiments.

Turbulence is often synonymous of (a) disordered motions, and (b) strongly diffusive features. In this context, (a) means that the specific motions that favor dynamo action maybe disrupted by the randomness of the flow. In addition, the small magnetic Prandtl number

values impose that the Joule resistive scale is very much larger than the hydrodynamic viscous length. It is therefore tempting to perform some kind of sub-scale average of the action of the turbulent velocity field. Then (b) leads to an effective magnetic diffusivity that could be much larger than the molecular value. These considerations have raised doubts on the very existence of fully turbulent dynamos [8].

One alternative is to engineer flow configurations that will preserve flow patterns which are essential for the dynamo generation. The design of the Riga and Karlsruhe experiments have been made to ensure that the time-averaged flow field resembles laminar flows which are kinematic dynamo solutions[1, 2]. These pioneering studies have validated the principle of a *fluid* dynamo, and have shown many fundamental dynamo properties. The threshold for dynamo action has been found to be in good agreement with predictions, showing the predominance of the large scales in their dynamo processes.

Another possibility, often explored in the geophysics community, is provided by strongly rotating flows. In this case, the Proudman-Taylor constrain may be able to prevent the development of strong three-dimensional turbulent fluctuations. This effect may even be strengthened by the generation of a dynamo dipole with its axis parallel to the rotation vector. Experiments in rotating Couette flows are studied in Grenoble and Maryland. Preliminary studies have not shown self-generation, but have pointed to the existence of *waves* in these strong rotating and magnetized flows: inertial, magneto-rotational, Alfvèn, etc. Their role regarding dynamo self-generation has yet to be elucidated.

The VKS experiments have shown that it is possible to generate a dynamo from fully turbulent motions. Its characteristics have not been predicted by studies based on the time-averaged flow pattern, although it is believed that helicity and differential rotation do play a leading role. The existence of fully turbulent motions has a major impact on the power requirements of the experiment. In the limit of very high R_V values, the hydrodynamic power consumption (below dynamo threshold) scales as $P = \rho L^2 U^3$ (ρ is the fluid's density), leading to magnetic Reynolds number $R_M = \mu\sigma(PL/\rho)^{1/3}$ (μ and σ are the magnetic permeability and electrical conductivity of the fluid, so that $\lambda = 1\mu\sigma$ is its magnetic diffusivity) . Engineering difficulties typically scale with the size L of the experiment, while operational costs are best associated with the power input P. Then, the above scaling shows that in order to reach high R_M values, one should use a fluid with the best electrical conductivity and lowest density (hence the use of liquid sodium), with size and power con-

sumption only contributing to the one-third power. $R_M \sim 10$ requires power inputs of the order 100 kW. As a result, it is easily realized that highly overcritical regimes will not be achieved in laboratory studies using conventional fluids [9]: experiments aim at reaching for the neighborhood of the threshold for dynamo onset. The above scaling $R_M(P)$ shows that highly supercritical regimes cannot be reached. In addition, it implies that once a geometry has been chosen, small variations in R_M^c can have a huge impact on the power or the size of the flow needed to reach self-generation. As a result, all experiments have been thoroughly optimized to have the lowest possible critical magnetic Reynolds number. This is a noteworthy peculiarity of the study of this hydromagnetic instability: energy and engineering constrains are such that one is not able to increase at will the control parameter of the instability; one must also choose conditions such that the thresholds is within the capacity of the selected setup. In this respect, the details of flow entrainment and the adjustement boundary conditions have been essential to all dynamo experiments so far.

We will first review the main induction processes that have been evidenced in fully turbulent MHD flows, before discussing the findings of dynamo experiments. We illustrate most features using measurements in the swirling flow generated in the gap between coaxial impellers inside a cylinder – the von Kármán flow geometry that we have studied using gallium or sodium as working fluid.

II. MAGNETIC INDUCTION AND DYNAMO ISSUES

Magnetohydrodynamics solves the coupled set of induction and momentum equations:

$$\partial_t \mathbf{B} = \nabla(\mathbf{u} \times \mathbf{B}) + \lambda \Delta \mathbf{B} \ , \tag{1}$$

$$\partial_t \mathbf{u} + (\mathbf{u} \cdot \nabla)\mathbf{u} = -\frac{\nabla p}{\rho} + \nu \Delta \mathbf{u} + \frac{\mathbf{j} \times \mathbf{B}}{\rho} + \mathbf{f} \ , \tag{2}$$

where $\lambda = 1/\mu_0 \sigma$ is the magnetic diffusivity of the fluid with density ρ, $\mathbf{j}$ the electrical current, and $\mathbf{f}$ is the forcing term (which may include Coriolis or buoyancy forces if rotation / convective effects must be included). Flows of liquid metals as considered in the experiments discussed here are incompressible so that the velocity and magnetic fields are divergence free. Boundary conditions correspond to no-slip for the hydrodynamic field (the velocity at the boundary is equal to the velocity of the boundary), with the magnetic boundary conditions set by the characteristics of the boundary (electrical conductivity σ_b, magnetic permittivity

μ_b). Magnetic boundary conditions can be implemented by setting continuity conditions at the surface, e.g. $[\mathbf{n}.\mathbf{B}] = 0$, $[\mathbf{n} \times \mathbf{B}] = \mu_0 \mathbf{j}_s$ where $\mathbf{n}$ is the normal to the surface, $\mathbf{j}_s$ are eventual surface currents and [.] stands for 'jump across the surface'. Alternatively, the induction equation can be extended to the entire domain (encompassing regions outside the flow – with the condition that $\mathbf{B} \to 0$ at infinity), and inhomogeneities are incorporated into Ohm's law:

$$\nabla \times \frac{\mathbf{B}}{\mu(\mathbf{r})} = \sigma(\mathbf{r})(\mathbf{E} + \mathbf{u} \times \mathbf{B}) \ , \tag{3}$$

where the magnetic permittivity and electrical conductivity depend on position. Taking the curl of the above equation yields the induction equation in an inhomogenous medium:

$$\partial_t \mathbf{B} = \nabla \times (\mathbf{u} \times \mathbf{B}) + \lambda \Delta \mathbf{B} - \nabla \times (\lambda \nabla \ln \mu \times \mathbf{B}) - \nabla \lambda \times (\nabla \times \mathbf{B}) \ . \tag{4}$$

with $\lambda = 1/\mu\sigma$, and it will be pointed out below that boundary conditions are essential for the interpretation of measurements of magnetic induction [5–7].

A. Induction processes

Despite efforts that are bow almost a century old, research has so far failed to establish sufficient conditions for dynamo action – some necessary conditions have been provided by anti-dynamo theorems. In this context, work has been aimed at uncovering efficient induction processes that could co-operate towards dynamo generation. In these studies an external field $\mathbf{B}^A$ is applied, and one analyses magnetic response, *i.e.* the induced field $\mathbf{B}^I$. For simplicity, the applied field is often homogeneous. We review in this section essential mechanisms that have been uncovered, with examples drawn from our own studies of the von Kármán flows generated inside a cylinder by the rotation of coaxial impellers, cf. figure 1. In these studies the applied field is low, so that the effect of the Lorentz force can essentially be neglected in the fluid's momentum equation. The magnetic response probes the structure of the velocity gradients and boundary conditions.

1. Shear and ω-effect

One mechanism is the shearing of magnetic field lines by velocity gradients, *i.e.* with $\mathbf{B}^I$ having its source in the $B^A \partial_A \mathbf{v}$ term of the induction equation, where $\partial_A \cdot$ stands for

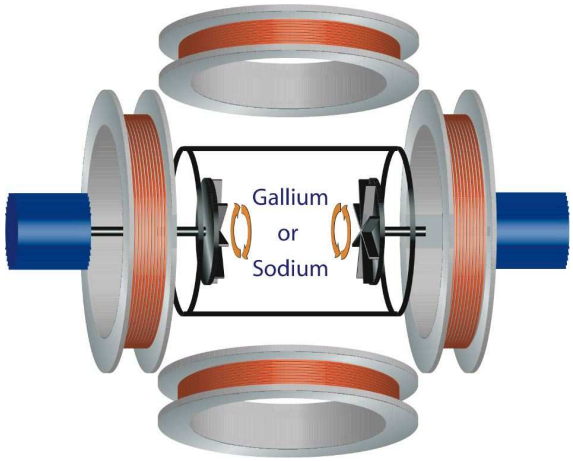

FIG. 1: Schematics of induction measurements in the von Kármán geometry [10]. Flows are generated by the independent rotation of 2 coaxial impellers (co- or counter-rotating) in a cylinder – the aspect ratio is one, with a cylinder diameter equal to the distance between the impellers. Depending on the configurations, the resulting mean flows have azimuthal and meridional profiles similar to the $s_{1,2}t_{1,2}$ types considered by Duddley and James [11] for dynamo generation. Note that these flows are strongly turbulent [12]; discussion in this section are restricted to the mean (time-averaged) features. External coils are set to applied either axial or transverse fields, and Hall probes inserted inside the flow vessel allow the measurement of the magnetic fields induced by the fluid motions.

'gradient along the A-direction'. For steady state conditions at low magnetic Reynolds number, the induction equation then leads to a linear dependance of B^I with R_M, a feature that can be used to estimate an intrinsic magnetic Reynolds number from experimental data as $R_M^I \equiv B^I/B^A$ [13]. This induction process is called the ω-effect when the velocity gradient comes from differential rotation, *e.g.* from a variation of a rotation rate along its axis. An example is provided in the von Kármán setup when the flow is driven by counter rotation of the impellers. A layer with differential rotation forms in the mid-plane and the twisting of axially applied magnetic field lines generates an azimuthal component – cf. Figure 2.

Another simple instance of this situation is when an electrically conducting plate rotates above a similar one at rest: if an external field is applied parallel to the axis of rotation, the differential rotation generates an induced field in the azimuthal direction. The solid rotor dynamo experiment devised in the 1960's by Lowes and Wilkinson is based on this principle [14]: it couples two such induction effects in an 'ω^2-dynamo'.

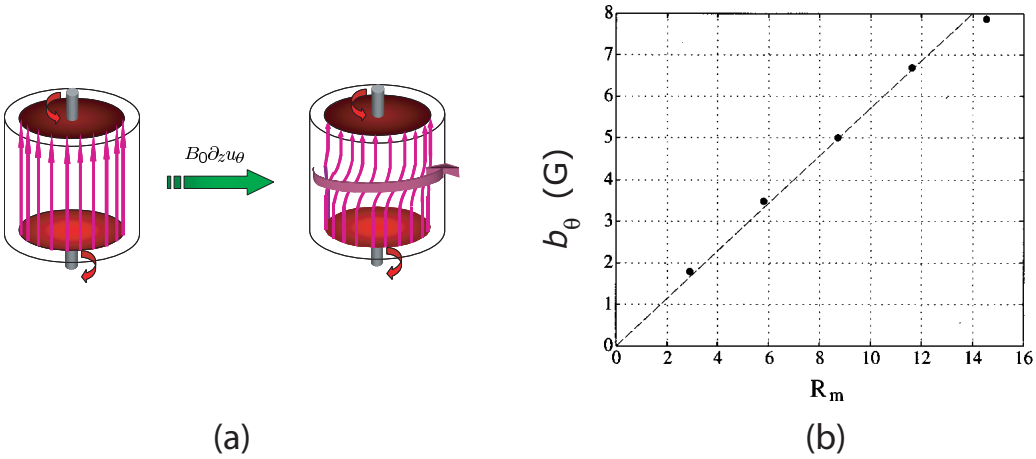

FIG. 2: Experimental verification of ω-effect in the von Kármán flow. Gallium is the working fluid. An axial magnetic field is applied with external Helmotz coils, and the azimuthal induced field is measured by a Hall probe in the mid-plane and inside the flow. Applied field 33 G. (a) sketch of the effect; (b) measurement of the induced field with $R_M = 2\pi R^2\Omega/\lambda$ – where R is the radius of the cylindrical vessel and Ω the rotation rate of the impellers. Plot from reference [**?**]

2. Helicity and the 'Parker-effect'

Another crucial mechanism is the 'stretch and twist' effect [15]: helical motions can deform initially straight magnetic field lines into loops which are associated with induced currents parallel to the applied field, $\mathbf{j}^I \propto \mathbf{B}^A$. This non-linear effect was first tested experimentally by Steenbeck [16] in an arrangement with interlaced channels – note that in this original setup the local helicity $h = \mathbf{u} \cdot (\nabla \times \mathbf{u})$ is strictly zero everywhere, so that the magnetic field diffusion is essential in this process.

This Parker-effect has also been observed directly in von Kármán experiments [17, 18]: the flow is generated inside a cylinder by the rotation of one disk at one end of the cylinder; it acts as a centrifugal pump so that fluid is drawn in a swirling motion along the cylinder axis. As expected the induced magnetic field varies quadratically with the flow velocity, $B^I \sim B^A R_M^2$ (dashed line in the measurements of figure 3). However, at high R_M values another effect sets in: the expulsion of the applied field from coherent eddies (see below) which causes a saturation in the Parker-induced magnetic field.

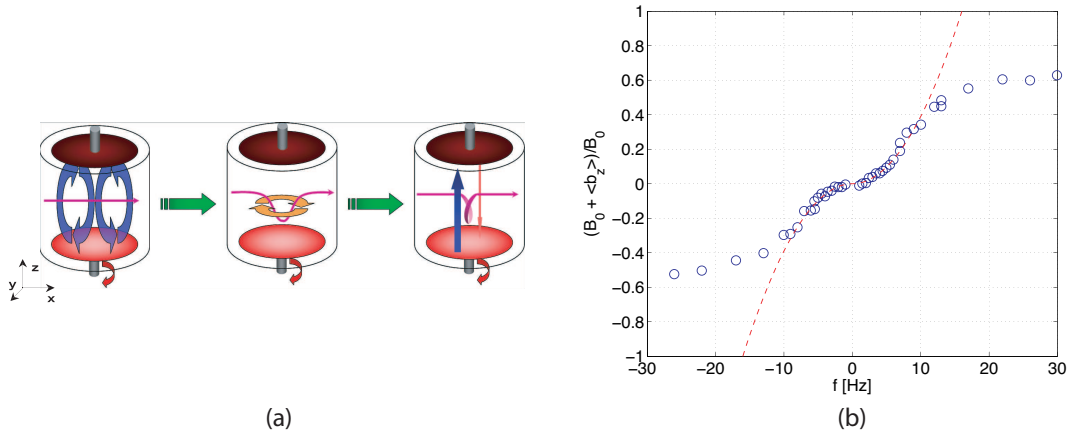

FIG. 3: Experimental verification of the Parker-effect in the von Kármán sodium flow. A magnetic field perpendicular to the cylinder (along the x-axis) is applied with external coils and the axial component of induced field is measured by a Hall probe inserted in the mid-plane, inside the flow. (a) sketch of the effect; (b) measurement of the induced field with the rotation rate of the impellers, from reference [17]. The dashed (red) line is a quadratic fit; departure at large rotation rates (> 10 Hz) is due to the expulsion of the applied field by the flow rotation.

3. Coherent vortex motion and expulsion

Rotational flow motion was involved in the two above examples of ω and Parker effects. However, another well-known effect is the expulsion of magnetic field lines from regions with closed stream lines [5](chapter 3). If a magnetic field is initially applied transverse to a coherent vortex, then closed loops form and decay in such a way as to gradually expel all magnetic flux from any region in which the streamlines are closed. This effect is related to the traditional skin penetration of conventional electromagnetism (in the reference frame rotating with the vortex). It is has been clearly evidenced in the von Kármán swirling flow with the impellers *co-rotating* so as to generate a coherent axial vortex [19].

A sketch of the effects and corresponding experimental measurements are shown in figure 4, taken from [21]. The field decays near the rotation axis, and correspondingly field lines are compressed outside of the vortex core.

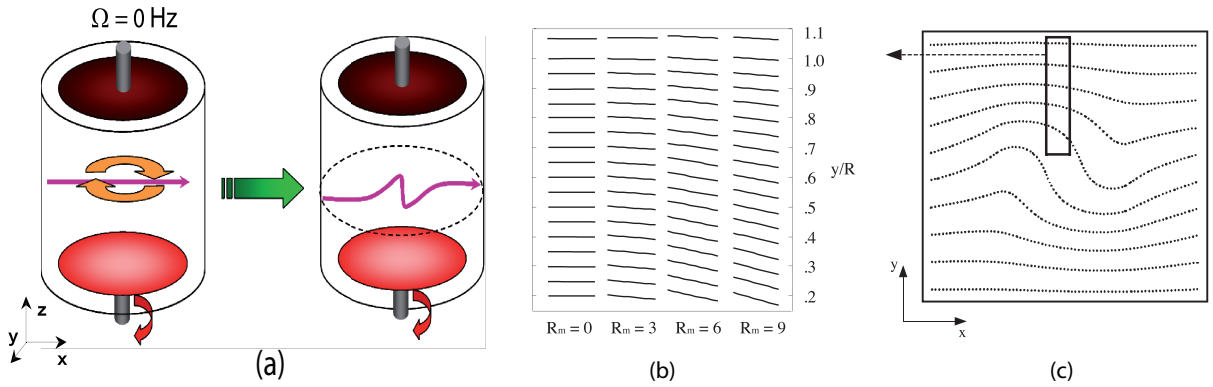

FIG. 4: Experimental verification of magnetic expulsion by coherent vortex motions. Gallium is the working fluid. A uniform magnetic field perpendicular to the cylinder (along the x-axis) is applied with external coils and the evolution of its orientaion along a radius is studied as the magnetic Reynolds number is increased. (a) Sketch of the torsion of the applied field lines; (b) evolution of magnetic field orientation in the measurement (the lines give the local direction of the magnetic field inside the vessel), from reference [21]; (c) equivalent numerical simulation from [20]. The boxed region is the one probed experimentally in (b), at increasing R_M values.

4. Electrical boundary conditions

Boundary conditions play an important role, particularly in the way induced currents flow in the system. As a result, induced magnetic field measured by a local probe come from an overall distribution of induced currents rather than from a local deformation of applied magnetic field lines. This can be clearly illustrated again using the von Kármán geometry with counter-rotating impellers and a transverse applied field – figure 5(a1). The deformation associated with differential rotation corresponds to an axial current sheet in the mid-plane, as in figure 5(a2,3). In turn, these currents generate induced field near the insulating boundary (shown in figure 5(a4)) at a right angle from the applied field [7, 18].

This effect, which source traces back to the $\nabla\lambda\times(\nabla\times\mathbf{B})$ term in equation (4), varies linearly with the magnetic Reynolds number as does its source – the differential rotation, and the effect has been accurately treated in several numerical simulations [22, 23, 45]. Inhomogeneities in the magnetic boundary conditions, which appear to favour dynamo action [59] have been considered in numerical studies [24, 25] but need to be probed in more details experimentally.

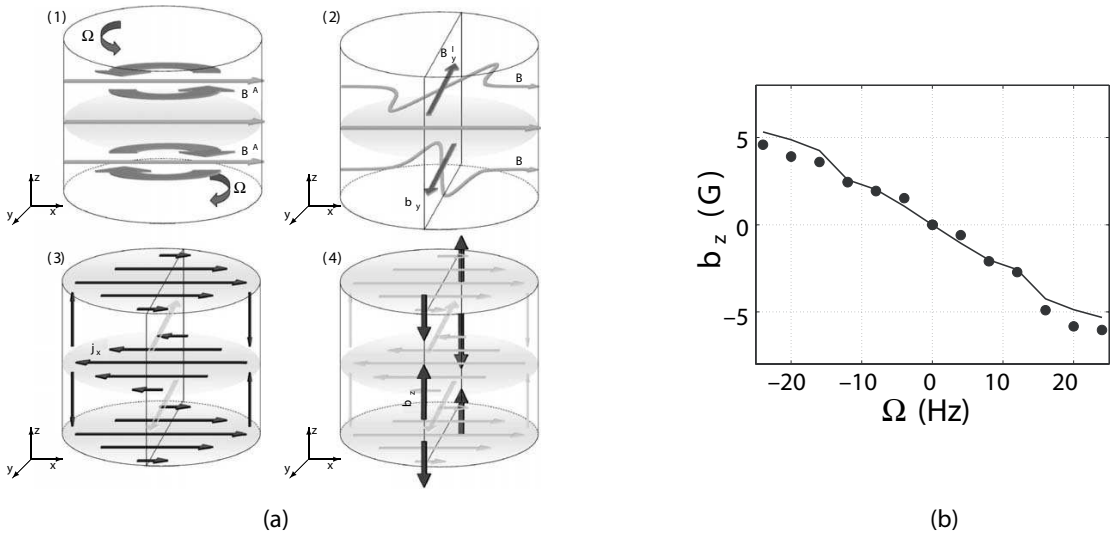

FIG. 5: Effet of boundary conditions. (a) Sketch of the BC-effect for a transverse applied field (33 Gauss) B^A along the x-axis in a counter rotating von Kármán flow : (1) initial field and discs rotations; (2) differential rotation creates an induced component B_y ; (3) induced current sheets responsible for the generation of B_y ; (4) axial field B_z generated at the wall $y = R$, due to the discontinuity in electrical conductivity. (b) Measurements of the induced axial magnetic field by BC-effect for a transverse applied fied along the x-axis with both counter-rotating discs in von Kármán experiment, from reference [18].

5. Discussion

The above induction mechanisms have been the building blocks of dynamo experiments so far – and this has motivated their presentation. A detailed discussion of induction in MHD is outside the scope of this review, but the following remarks may be helpful in regards to experimental investigations:

- At low R_M, induction is linear in the velocity gradients and can thus be used to probe them. This is a very useful feature for the study for hydrodynamics in liquid metals, for which velocimetry techniques are not as well developed as for conventional liquids. For instance, it has recently been used in the Grenoble and Maryland experiments for the study of waves in spherical Couette flows [26].

- Induction from uniform applied field may mask non-local features of the induction process, for which magnetic field advection is as important as line deformation. In addition, the presence of the Laplacian term in the induction equation performs some kind of averaging since

at low P_M the resistive scale is much larger than the turbulence viscous cut-off. Advection effects from localized magnetic field sources have been studied in the VKS experiment [28]; field transport can reach distances larger than the flow integral scale and cause significant magnetic intermittency when turbulence is present.

- It has been observed in several instances (cf. [29]) that the induced magnetic field within the flow can reach values higher than the applied field. However, these situations were not necessarily associated with dynamo self-generation. In other words, flows can have very efficient field amplification factors without dynamo property (an analytic example is the case of a plane flow with diverging streamlines from a point source which would strongly amplify any toroidal magnetic field). In fact, an experimental criterion for the proximity of a dynamo threshold is still lacking. The decay time of applied magnetic field pulses has been studied by the Maryland group [30], but in conditions where dynamo generation was not reached so it is not yet known how theses decay time would diverge near onset and how.

B. Mean-field MHD

We now discuss separately the case of the mean-field MHD approach and its consequences. The reason is that it proposes an efficient treatment of the effects of turbulence and that it has been very successfully used in the modelling of stellar dynamos – e.g. [33]. There has thus been some strong motivation to test it experimentally.

We first recall the basics of mean-field MHD, readers being referred to [5, 31, 32] for a more complete presentation. One splits the velocity and magnetic fields into an ensemble average and a fluctuating component: $\mathbf{u} = \overline{\mathbf{u}} + \mathbf{u}'$ and $\mathbf{B} = \overline{\mathbf{B}} + \mathbf{B}'$,

$$\partial_t \overline{\mathbf{B}} = \nabla \times (\overline{\mathbf{u}' \times \mathbf{B}'}) + \nabla \times (\overline{\mathbf{u}} \times \overline{\mathbf{B}}) + \lambda \Delta \overline{\mathbf{B}} \ , \tag{5}$$

where the mean electromotive force $\mathcal{E} = \overline{\mathbf{u}' \times \mathbf{B}'}$ can be computed after solving the equation for the fluctuating part of the magnetic field:

$$\partial_t \mathbf{B}' = \nabla \times (\mathbf{u}' \times \mathbf{B}') - \nabla \times \mathcal{E} + \nabla \times (\overline{\mathbf{u}} \times \mathbf{B}') + \nabla \times (\mathbf{u}' \times \overline{\mathbf{B}}) + \lambda \Delta \mathbf{B}' \ . \tag{6}$$

In the above equation, one then usually invokes scale separation between flow sizes at which velocity gradients are effective and the global scale at which magnetic effects are considered. One then makes the assumption that the mean e.m.f. can be expanded in terms of the mean

magnetic field $\overline{\mathbf{B}}$ and its spatial derivatives. For very general situations in the presence of a mean flow this is quite a complex task, often guided by symmetry considerations [32]. Usually, the first two terms of the expansion are retained, corresponding to
- the so-called alpha-effect, *i.e.* the possibility to generate induced currents which are parallel to the large scale field, via an emf $\mathcal{E} = \alpha(\mathbf{u})\overline{\mathbf{B}}$. For instance, such current have the ability to generate a poloidal magnetic field from an azimuthal one (as cooperative Parker effect from small scales), a very interesting feature for the modelization of natural dynamos.
- the 'beta-effect', which corresponds to a contribution to the induced mean emf related to the gradients of $\overline{\mathbf{B}}$, $\mathcal{E} \propto \beta(\mathbf{u})(\nabla \times \overline{\mathbf{B}})$. This term represents a potential additional diffusion of the magnetic field, over the molecular Joule effect.

In cases where the flow geometry is prescribed in a simple enough form, the α term can be computed analytically. This is the case computed by Roberts [34], for a flow consisting of an array of columns in which the motions are helical with alternate axial and angular velocities, but unchanged helicity. This effect is the basis of the Karlsruhe dynamo experiment [35, 36], for which both the scale separation and the helical nature of the flow are enforced by the design of the tubes which guide the flow. One can thus conclude that a cooperative effect of small-scale helical motions is experimentally observed in situations where the helical motions are strictly enforced.

The picture is somewhat different in flows where helicity evolves freely. For homogeneous (but not mirror-symmetric) turbulence, α can be computed in terms of the helicity spectrum of the flow [5]. For more complex geometry (in particular when mean flow motions are also present) a formal derivation of the α tensor has been performed using symmetry arguments [32]. Some contributions have been tested experimentally in the Perm spin-down experiment [39, 40], figure 6(a): liquid Gallium is spun inside a torus which is suddenly halted; as the liquid moves with respect to the vessel, it flows past mechanical diverters which impart a global screw motion – then helicity is often assumed to cascade down to smaller scales [41]. Analysis of the magnetic field induced by an applied toroidal field is shown in figure 6(b) where the induced field is monitored in the spin-down regime **??**. The α value measured experimentally is much lower than predictions derived by the mean-field theory. In addition, the main contribution traces back to the large scale inhomogeneity of the velocity gradients, rather than to the small scale helicity distribution.

Direct measurements of the β effect have been performed in two experiments. In a first

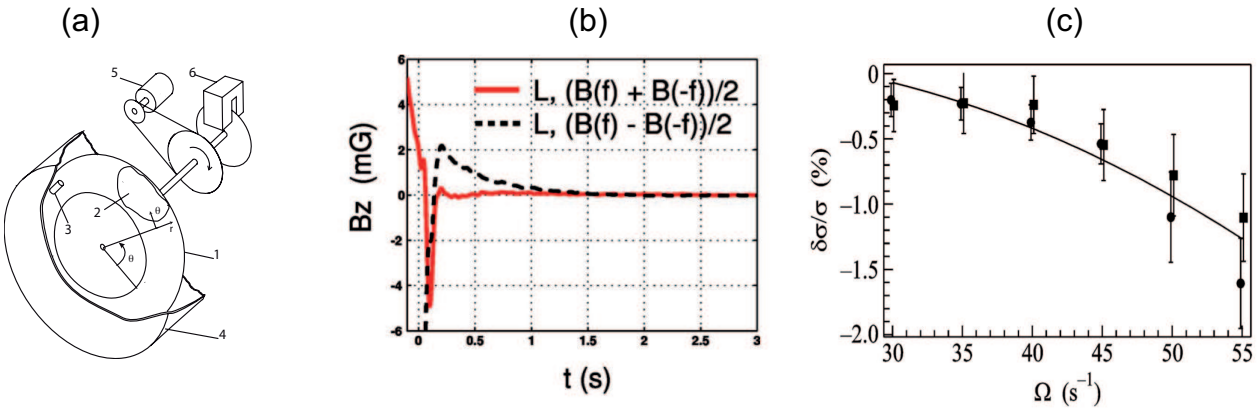

FIG. 6: Investigation of mean-fied contributions. (a) Sketch of the Perm torus experiment (1: vessel, 2: test section, 3: Hall probe, 4: external shield, 5: motors, 6: braking device). (b) Study of possible α-mechanisms: response to a DC applied field with its direction parallel to the large scale helicity in the spin-down regime: the red curve has the symmetry of the alpha effect and is concentrated during the initial phase of motion, while the black dashed curve is the linear induction and follows the flow decay – figure from [42]. (c) Study of possible β effect, using the induction from an AC applied field. The plot shows the change in effective electrical conductivity with the initial rotation rate of the torus, from reference [44].

one at very moderate turbulent Reynolds number, an increase of the molecular diffusion by a few percent has been claimed [43]. A more recent, and far more detailed experimental study, has been performed by the Perm group. It show a correction to the molecular magnetic diffusivity of 1% at most [44] – figure 6(c). The scaling with magnetic Reynolds number was found to be in agreement with mean-field theory expressions, but the amplitude again much smaller than predicted. Finally, an indirect estimation of the effect of turbulence on magnetic diffusivity is provided by the dynamo onset in the Karlsruhe and Riga experiments: in both cases the threshold was found to be in excellent agreement with predictions based on a laminar mean flow, *i.e.* neglecting small-scale turbulent fluctuations. The field at saturation however, was observed to be in good agreement with a balance of the Lorentz force by the turbulent fluctuations (inertial term) [69].

There is thus experimental indications that for flows of liquid metals at moderate magnetic Reynolds numbers, the effects that can be attributed to small-scale turbulence are actually smaller than predicted by the mean-field MHD theory. It does not mean that tur-

bulence does not play a role in experimental dynamos. On the contrary, we will show that the VKS dynamo cannot be attributed to the mean (time-averaged) flow motions. In addition, induction measurements made in the Madison experiment [46] have directly evidenced the existence of a turbulent emf: an induced dipole moment has been measured in response to an axisymmetric magnetic field – with Cowling's theorem [47] showing that it cannot be attributed to axisymmetric flow motions. These are indications that, at least for low P_M fluids, the turbulent and non-stationary fluctuations in the vicinity of the large scales may play a dominant role in the induction processes.

C. A synthetic dynamo

We conclude this section with an example of a dynamo based on an arrangement initially proposed by Bullard [48], and in which the dynamo cycle is viewed as a series of magnetic induction steps. An initial magnetic seed field $\mathbf{B}_0$, transported and stretched by the velocity gradients gives rise to an induced magnetic field component $\mathbf{B}_1$, which in turn generates an induced field $\mathbf{B}_2$, etc. until eventually the contribution after n steps $\mathbf{B}_n$ reinforces $\mathbf{B}_0$ [45]. If this feedback process is efficient enough, $\mathbf{B}_0$ is self-sustained (it is the neutral mode of the dynamo instability).

In the spirit of Bullard's design, we use the differential rotation in the von Kármán flow with two counter rotating disks. It advects and stretches an externally applied axial field B_z, generating a toroidal component B_θ. This induced field is used to drive a power source which generates the current in the Helmholtz coils creating B_z – cf. figure 7. Hence, part of the dynamo cycle is generated by an external feed-back: one prescribes the mechanism by which a toroidal magnetic field generates an induced poloidal one. The feedback loop from the induced toroidal field to the applied axial one has an adjustable gain which selects the magnetic Reynolds number for dynamo onset. The flow turbulence is included in the poloidal to toroidal conversion (ω-effect) and has a leading role. Another feature of this arrangement is that saturation of the dynamo is not at present reached after a modification of the flow field, but rather when the source of electrical current in the external coils has reached its limit value $I_{\max}$. The effect of turbulence are thus best isolated in the vicinity of onset [50, 51]:

(i) the bifurcation to dynamo proceeds via an on-off scenario,

(ii) the birfurcation is very much dependent on the geometry and dynamics of the von Kármán flow fluctuations. Both homopolar or reversing dynamos have been observed depending on the presence of additive noise in the induction process – see figure 7. This is in agreement with recent models of on-off bifurcations [52].

III. DYNAMO EXPERIMENTS

A. The Riga experiments

The arrangement in Riga is inspired by the Ponomarenko kinematic dynamo [53, 54], generated by the helical motions in an infinite stationary conductor. With the first experiments made in the 80's, this swirling flow configuration has been thoroughly optimized [55]: back flow characteristics, addition of an external layer of sodium at rest, length of the main channel, poloidal to toroidal velocity ratio, etc. Generation and saturation of a time-dependent

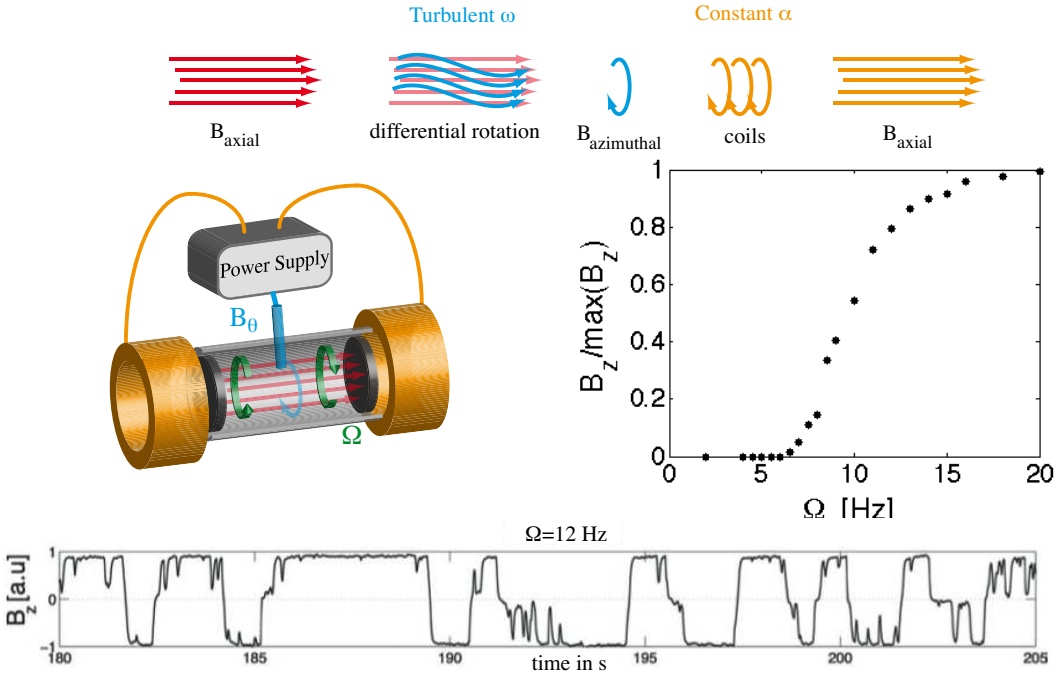

FIG. 7: The Bullard von-Kármán dynamo. (top): principle of dynamo feed-back loop with actual implementation (middle left). The mid-right curve is the bifurcation curve of the self-sustained magnetic field as the rotation rate of the impellers increase. The bottom figure shows an example of time signal, with spontaneous reversals of the dipole field, figure from [50].

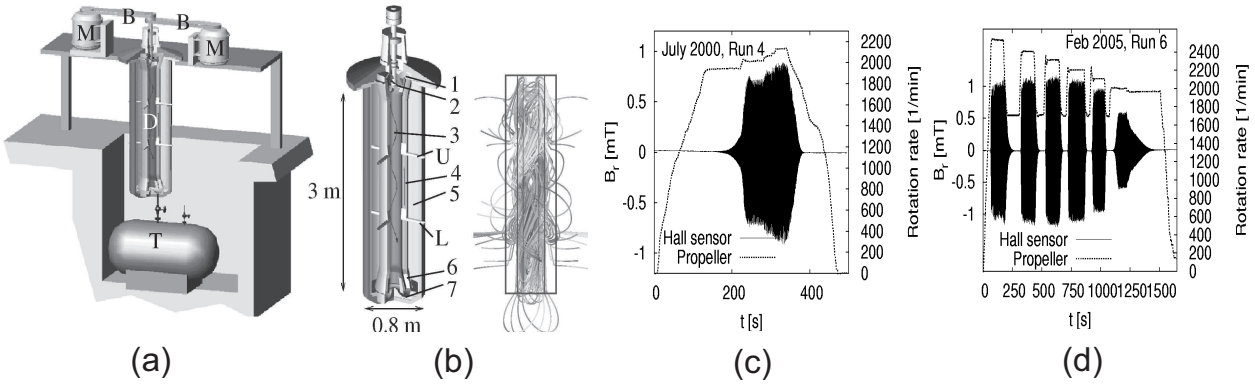

FIG. 8: The Riga dynamo experiment and its neutral mode. (a) Sketch of the facility. M - Motors. B - Belts. D - Central dynamo module. T- Sodium tank. (b) Sketch of the central module. 1 - Guiding blades. 2 - Propeller. 3 - Helical flow region without any flow-guides, flow rotation is maintained by inertia only. 4 - Back-flow region. 5 - Sodium at rest. 6 - Guiding blades. 7 - Flow bending region. Associated simulated magnetic eigenfield. The gray scale indicates the vertical components of the field. (c) and (d): Two experimental runs carried out in July 2000 and in February 2005. Rotation rate of the motors, and magnetic field measured at one Hall external sensor plotted vs. time. Figures from reference [3](figs.5& 6).

dynamo was first observed during summer 2000.

For a fluid in axial translation at velocity U_z while rotating at speed U_θ in a cylinder of radius R, the threshold for (Ponomarenko) self-generation in magnetic Reynolds number $R_M = R\sqrt{U_\theta^2 + U_z^2}/\lambda$ is $R_M^c \sim 17.7$, and the bifurcation is a Hopf one: the magnetic field at onset is oscillatory. This is very close to the threshold (17.6) observed in the experiment, with the additional following observations [56]:

- optimization studies have shown that lowest threshold values are obtained when $U_\theta/U_z \sim 1$, *i.e.* for a unit ratio of 'poloidal' to 'toroidal' velocities – a feature common to all dynamo experiments so far,
- the layer of sodium at rest around the flow leads to a decrease in R_M^c,
- the main mechanism of magnetic field saturation lies in the braking of the azimuthal velocity component, so that differential rotation (with respect to the stationary outer medium) and thus field amplification are reduced.

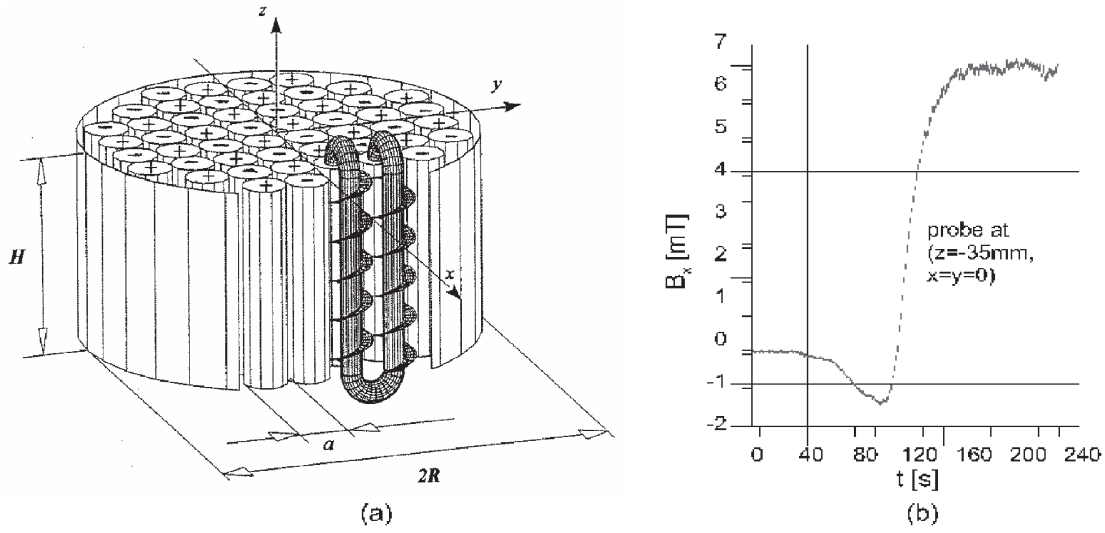

FIG. 9: The Karlsruhe dynamo experiment. (a) Central part of the facility. The module consists of 52 spin-generators, each containing a central tube with non-rotating flow and an outer tube where the flow is forced on a helical path. (b) Self-excitation and saturation in the Karlsruhe dynamo experiment. Hall sensor signals of Bx in the inner bore of the module. Figure taken from reference [3].

B. The Karlsruhe experiment

Like the previous one, the Karlsruhe experiment is designed to replicate a velocity field with a topology that is known to generate a dynamo. Here, the flow field traces back to a calculation by G.O. Roberts [34] for a period array of vortices with the same helicity. This arrangement was later adapted by F. Busse for possible scenarii of the Earth dynamo, a possibility that motivated the Karlsruhe experiment. In practice each helical vortex is made of 2 concentric channels: one in which the flow is purely axial, and a surrounding one in which the fluid is guided in helical motion.

A very comprehensive review of the experiment and its findings can be found in [58]. The actual experiment involves 52 screw-flow generators, and dynamo action was obtained for critical values of the magnetic Reynolds number $Rm^c = \alpha_\perp L/\lambda \in [8.4, 9.3]$ (here the α parameter is used as a velocity characteristic scale, and L is the overall cross-section of the experiment). This is again very close to the value (8.2) predicted using several approaches based on a laminar flow structure [57]. The bifurcation is supercritical, with a (statistically) stationary magnetic field generated at onset. The magnetic field generated is of dipolar

character, oriented perpendicular to the axis of the spin generators ('an equatorial dipole'). Measurement of the pressure and flow rates in the channels indicate an additional dissipation above onset which varies linearly with the flow rate, with an order of magnitude of about 10 kW at 10% over threshold [58]. As the dynamo field grows, a reduction of the flow velocity in the spin generators is also observed, however, the detailed mechanisms of the saturation of the instability are not known.

C. VKS experiment

The Karlsruhe and Riga experiments have validated the principle of fluid dynamos. In each flow the kinetic Reynolds number is huge, but the overall behavior is in good agreement with the predictions of quasi-laminar approximations. They have shown that the dynamo generation is controlled by the topology and dynamics of the large scale flow. Secondary bifurcations or more complex magnetic regimes have not been observed. The VKS experiment has been designed designed to keep essential ingredients (shear and helicity) while at the same time allowing for more freedom to the hydrodynamics flow – and hence to the magnetic field dynamics.

The flow is generated by rotating two impellers inside a cylindrical copper vessel – details are given in figure 10. The impellers can be independantly driven up to typically 27 Hz by motors with 300 kW available power. When both impellers rotate at the same frequency $F_1 = F_2$, the forcing is symmetric with respect to any rotation R_π of π around any radial axis in its equatorial plane ($x = 0$). Otherwise, when $F_1 \neq F_2$, the system is no longer R_π-symmetric. For simplicity, we will also refer these situations as 'symmetric/asymmetric' cases.

1. A statistically steady turbulent dynamo

For symmetric forcing, one observes that as the rotation rate of the impellers $F = F_1 = F_2$ is increased above 17 Hz, the magnetic field inside the flow develops strong fluctuations and its main component (in the azimuthal direction at the probe location) grows and saturates to a mean values up to 100 G – figure 11. This value is about 100 times larger than the ambient magnetic field in the experimental hall, from which the flow volume is not shielded.

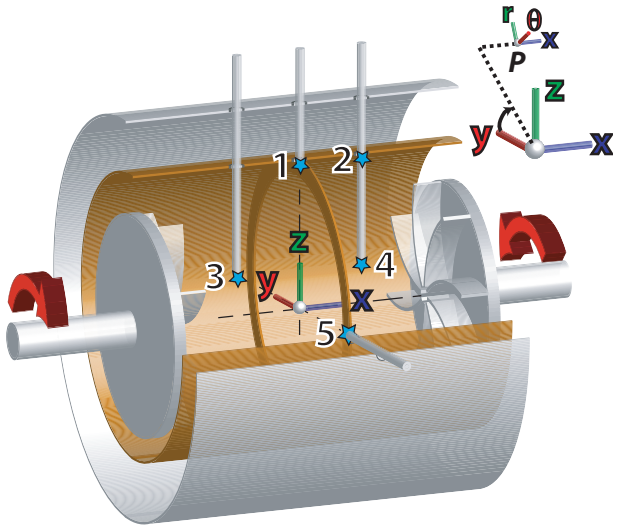

FIG. 10: Sketch of the VKS flow configuration. The flow is generated by rotating two impellers of radius 154.5 mm, 371 mm apart in a thin cylindrical copper vessel, $2R = 412$ mm in inner diameter and 524 mm in length. The impellers are fitted with 8 curved blades of height $h = 41.2$ mm; in most experimental runs, the impellers are rotated so that the blades move in a non-scooping direction, defined as the positive direction by arrows. The flow is surrounded by sodium at rest contained in another concentric cylindrical copper vessel, 578 mm in inner diameter and 604 mm long. An oil circulation in this thick copper vessel maintains a regulated temperature in the range $110 - 160°$C. In the mid plane between the impellers one can attach a thin annulus inner diameter 350 mm and thickness 5 mm. The impellers that generate the flow have been machined from pure soft iron ($\mu_r \sim 100$). Positions 1 to 5 correspond to points where time recordings of the magnetic field have been made, using 3D Hall probes. Figure from reference [64].

The hundred-fold increase is also one order of magnitude larger that the induction effects and field amplification previously recorded in the VKS experiment with externally applied magnetic field, either homogeneously over the flow volume [67] or localized at the flow boundary [68]. The most salient features of the dynamo observed with a symmetric forcing are the following [59, 62, 64]:

- it appears via a supercritical bifurcation at $R_M^c \sim 32$, generating a statistically steady magnetic field,
- the geometry of the dynamo field is mainly that of an axial dipole,
- opposite polarities of the dipole have been observed as R_M is increased above threshold (in

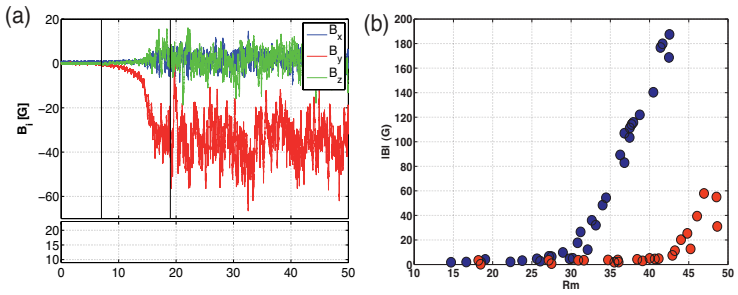

FIG. 11: Self-generation in the VKS experiment. (a) Growth of the magnetic field as the rotation rate of the impellers $F = F_1 = F_2$ is increased from 10 to 22 Hz. Three components of the magnetic field recorded at location 1. (b) magnetic field amplitude $\langle B^2 \rangle^{1/2}$recorded at location 3; (blue circles): counter-rotating impellers at equal rotation rates, in the positive direction shown in figure 9. (red circles): impellers counter-rotating in the opposite direction, i.e. with the blades on the impellers moving in a scooping or negative direction. Changes in the efficiency of the stirring are taken into account in the definition of R_M; $R_M = K\mu_0\sigma R^2 F$ with $K = K+ = 0.6$ in the normal, positive direction of rotation and $K = K- = 0.7$ in the opposite direction. Figure from reference [64].

agreement with the expected $\mathbf{B} \rightarrow -\mathbf{B}$ symmetry of the equations) but once a direction of the dipole has been chosen at onset, no secondary bifurcation is observed as R_M is increased to its maximum accessible value ($R_M^{\max} \sim 50$),

- the amplitude of the field at saturation is in good agreement with a balance of the Lorentz force with the non-linear term in the Navier-Stokes equation [69].

The observation that the magnetic field geometry for the symmetric VKS forcing is mainly dipolar has important implications. It strongly differs from the prediction of kinematic calculations based on the topology of the mean von Kármán flow which tends to favor a transverse dipole [45, 65, 66]. In addition, Cowling theorem [5] implies that it has not been generated by the mean flow motions alone. The axial symmetry, however, is what would be expected from an $\alpha - \omega$ dynamo. The differential rotation induced by the counter-rotation of the impellers has the ability to generate an azimuthal field component from an axial magnetic field [18, 67]. The conversion by the α-effect of a toroidal field into a poloidal one is often thought to rely on helical flow motions, but the source of the α term in VKS is yet unclear. Several mechanisms have been proposed [64] and further measurements are

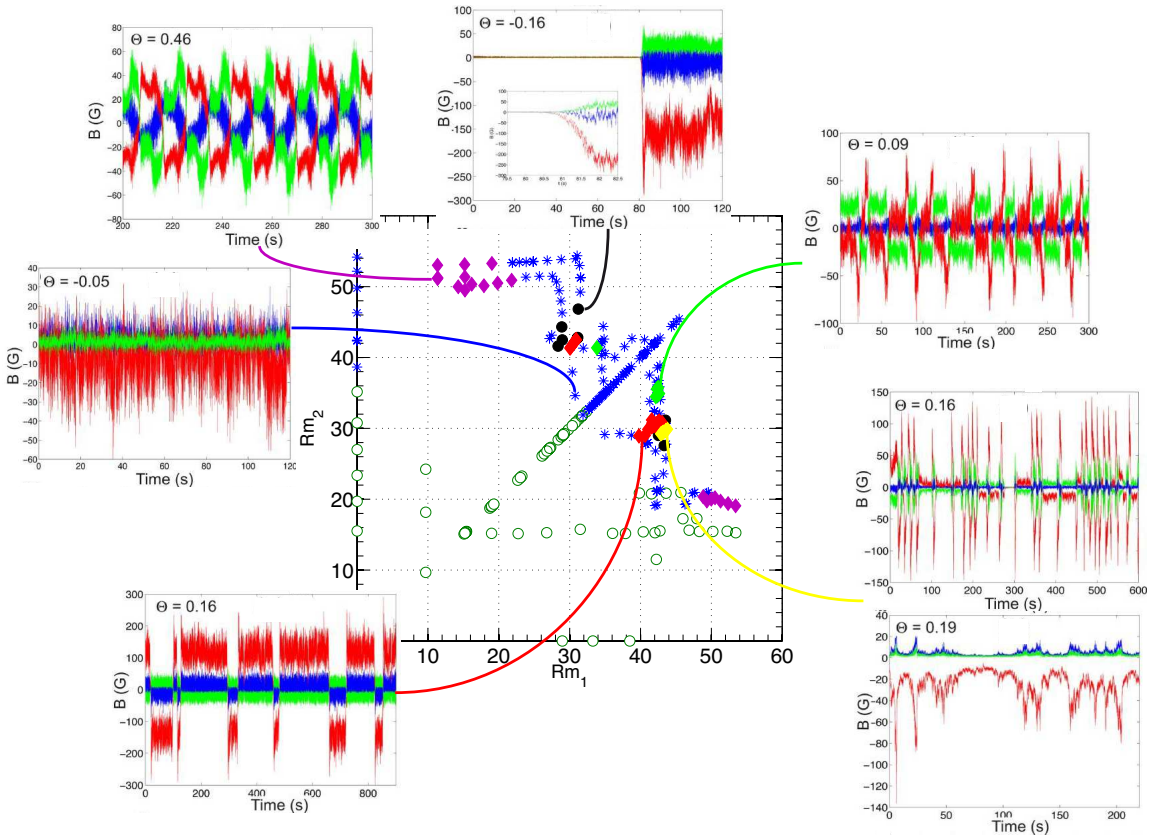

FIG. 12: Dynamical regimes observed in the von Kármán sodium experiment when the impellers driving the flow rotate at varying rates: the coordinates in the main plat are the magnetic Reynolds numbers built from the velocity of each impeller. The insets give examples of time signals of the 3 components of the magnetic field recorded in the mid-plane of the cylinder. Figure extracted from data in reference [64].

underway.

2. *Dynamical regimes for an asymmetric forcing*

When the flow is forced with the impellers rotating at different rates, studies in water-propotypes have shown that global rotation is imparted to the flow [70, 71]: there are strong similarities between the von Kármán flow forced by impellers rotating respectively at F_1 and F_2 in the laboratory frame or by impellers rotating at $(F_1 + F_2)/2$ in a frame rotating at $(F_1 - F_2)/2$. In addition, this asymmetric differential forcing brakes the R_π symmetry.

The added degree of freedom gives access to a variety of dynamos with complex dynamical

regimes – they are shown in figure 12 using two independent Reynolds numbers built on the rotation rates of each impeller [64]. Regions where (statistically) stationary dynamos are generated alternate with regions for which the magnetic field is time dependent. Of particular interest is the region near $|\theta| \equiv 2|F_1 - F_2|/(F_1 + F_2) = 0.16$ where reversals of the dipole field are observed at irregular time intervals. This regime, which also includes excursions, bears some similarity with the behavior of the geodynamo [60]. Another very intriguing regime is reached in the same region where the dynamo has sudden 'bursts' between high and low fields states - figure 12(right part). Both regimes are observed in a region where the flow has also two possible states [61].

Further studies [63] have shown that these regimes can be interpreted as the development and interaction of few dynamo modes (essentially a dipole and a quadripole) when the flow is forced asymmetrically. The proximity of dipole and quadrupole modes in $\alpha - \omega$ dynamos has been pointed out by many numerical studies [72], and few-modes interactions have long been used to ascribe dynamical features to the dynamo instability [73]. For the case of the VKS dynamos, the onset of oscillatory behavior, the occurence of random reversals, have recenlty been described using a low dimensional model [74].

D. Related dynamo experiments

Several other experiments are operated or in preparation world-wide.

- A setup similar to the VKS arrangement, but in a spherical volume, is studied by the group of Cary Forest at University of Wisconsin (USA). It has shown the possibility that turbulent motions induce an axial dipole from an applied external field [46].

- The Complex Dynamics group headed by Daniel Lathrop at University of Maryland (USA) has operated a large variety of sodium experiments, showing in particular the influence of the driving on the induction efficiency [30]. The most recent developments have been made in cylindrical Couette flows with applied magnetic fields, showing flow evolutions consistent with a magneto-rotational instability [75]. A large spherical Couette experiment (with an outer sphere 3 meters in diameter) is planned; it will reach the highest accessible magnetic Reynolds numbers of all current experiments.

- A spherical Couette experiment is run in Grenoble (France)by the group of H.-C.

Nataf, D. Jault and Ph. Cardin. The inner sphere contains a strong permanent magnet with the purpose of studying flows and magnetic regimes in conditions closer to the one which prevail in the Earth. The first measurements have evidenced a large variety of magneto-inertial waves [76].

- At Institute of Continuous Media Mechanics in Perm (Russia), the team of Peter Frick has designed a spin-down helical flow inside a torus [39, 40]. Compared to other experiments the flow is strongly non-stationary: a strongly anisotropic turbulence

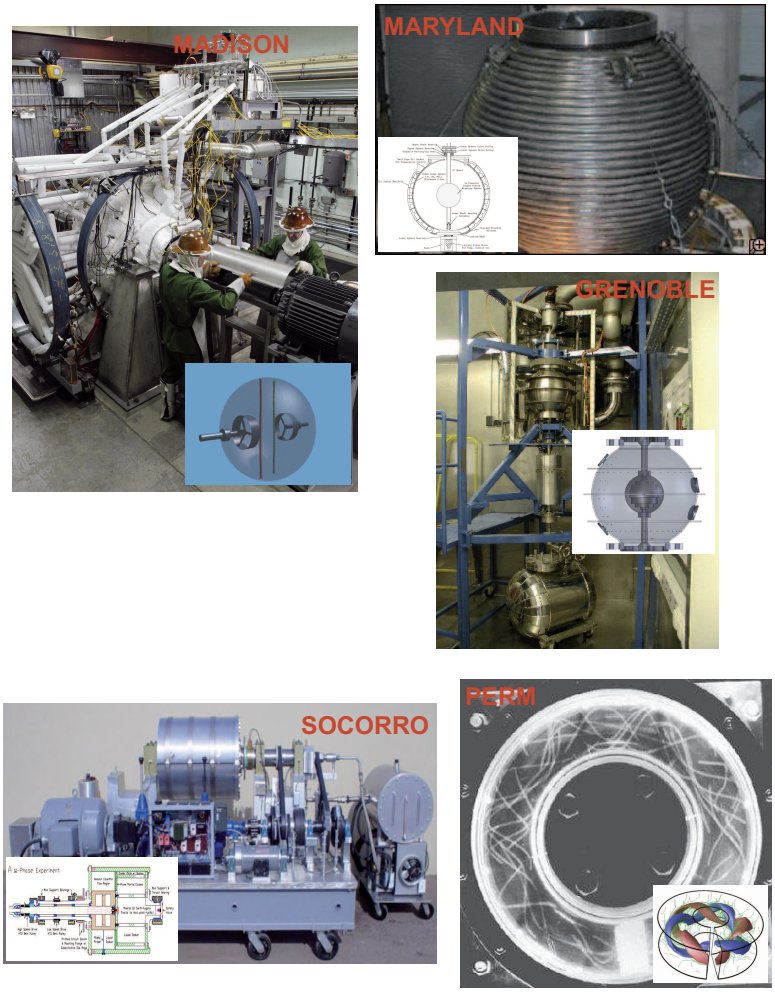

FIG. 13: Other sodium experiments operated or in preparation, aimed at studying the dynamo instability. Starting from top/left and clockwise: the Madison dynamo experiment at Univ. Wisconsin, USA; the 3-Meter system being installed at University of Maryland, USA; the DTS spherical Couette flow of the Grenoble team, France; the spin-down helical flow in the Perm torus, Russia; the cylindrical Couette flow In Socorro, New Mexico, USA.

develops and decays, as the fast-rotating torus is suddenly put to halt [77]. This flow has the potential to sustain a dynamo in the transient relaxation, and repeated realizations are expected to help understand the magnetic - velocity field interactions during the phases of growth, saturation and decay.

- In Socorro (New Mexico, USA), the team led by Sterling Colgate has designed a Couette flow operated with sodium, with the aim of generating an $\alpha\omega$ dynamo. Characterization of hydrodynamic flow transition have been carried out [79].

There are also several sodium experiments intended to study the Magneto-Rotational Instability (MRI) in Couette flows. One is developed in in Obninsk (Russia), in collaboration with the Kurchatov Institute in Moscow [80]. Another is in Rosendorf, operated by the group of Gunther Gerbeth and Franck Stefani. This experiment has recently shown an MRI in the form of a travelling wave [81]

IV. CONCLUDING REMARKS

Several features are shared by experimental dynamo operated so far with progressively less contrained motions – since the pioneering works of Lowes and Wilkinson in Cambrige in the 60's. All have observed that the bifurcation is supercritical, and subcritical bifurcation are yet to be evidenced experimentally. Boundary conditions have been essential, particularly in order to shift the critical magnetic Reynolds number R_M^c within the range accessible in the chosen experimental devices. Much further studies are necessary in order to understand the role of turbulence in the generation of the magnetic field and its saturation. With a growing number of dynamo experiments worldwide, and with the narrowing gap with numerical simulations, the next decade appears very promising.

Acknowledgements

Bullard - von Kármán experiments are operated at ENS-Lyon. The von Kármán Sodium experiments are designed and run by the VKS collaboration on the premises of the CEA-Direction de l'Energie Nucléaire in Cadarache. The VKS team includes François Daviaud, Arnaud Chiffaudel, Sébastien Aumaître, Bérengère Dubrulle, Florent Ravelet, Romain Monchaux, Louis Marié at CEA - Département de Sciences de la Matire; Stephan Fauve, François Pétrélis, Nicolas Mordant, Michael Berhanu at Ecole Normale Supérieure de Paris and Jean-François Pinton, Philippe Odier, Mickael Bourgoin, Romain Volk, Nicolas Plihon at Ecole Normale Supérieure de Lyon. Fruitful discussions with members of the VKS team are gratefully acknowledged.

This work was supported by CEA, CNRS and ANR NT05-1 42110 & ANR-08-BLAN-0039-02.

[1] MHD dynamo experiments, special issue of *Magnetohydrodynamics* **38**(1/2) (2002)

[2] The dynamo effect, experimental progress, geo and astrophysical challenges, *Comptes Rendus de l'Académie des Sciences* **9**(7) (2008)

[3] Stefani et al. Magnetohydrodynamic experiments on cosmic magnetic elds. *Zeitschrift fur Angewandte Mathematik und Mechanik* (2008)

[4] F., Petretlis, N. Mordant, S. Fauve, On the magnetic fields generated by experimental dynamos, *Geophys. Astrophys. Fluid Dyn.* **101**(3-4), 289 (2007)

[5] H. K. Moffatt, Magnetic Field Generation in Electrically Conducting Fluids, *Cambridge University Press*, Cambridge, (1978)

[6] Bullard E. C. and Gubbins D., *Geophys. Astrophys. Fluid Dyn.* **8**, 43 (1977)

[7] M. Bourgoin, Etudes en magnétohydrodynamique, application à l'effet dynamo, *PhD Thesis*, Ecole Normale Supérieure de Lyon (2003), `http://tel.archives-ouvertes.fr/tel-00008302/en/`

[8] A.A. Schekochihin, E.L. Haugen, A. Brandenburg, C. Cowley, J.L. Maron, J.C. McWilliiam, The onset of small scale turbulent dynamo at low magnetic Prandtl numbers, *Astrophys. J.***625**, 115 (2004)

[9] The development of experiments using plasmas as working fluids has recently been suggested by Cary Forest; they will lead to MHD studies at high R_M and P_M values.

E. J. Spence, K. Reuter, C. B. Forest, A Spherical Plasma Dynamo Experiment, `arXiv:0901.3406`

[10] P. J. Zandbergen and D. Dijkstra, *Annu. Rev. Fluid Mech.* **19**,465 (1987), and references therein.

[11] N. L. Dudley and R. W. James, *Proc. R. Soc. London*, Ser. A **425**, 407 (1989)

[12] Mordant N, Pinton JF, Chilla F. Characterization of turbulence in a closed flow, *J. Phys. II (France)* **7**(11), 1729 (1998)

Pinton JF, Plaza F, Danaila L, Le Gal P., Anselmet F., On velocity and passive scalar scaling laws in a turbulent swirling flow, *Physica D* **122**(1-4), 187 (1998)

Volk R, Odier P, Pinton JF, Fluctuation of magnetic induction in von Karman swirling flows, *Phys. Fluids* **18**(8), 085105 (2006)

[13] A. Martin, P. Odier, J.-F. Pinton, S. Fauve : Effective permeability in a binary flow of liquid gallium and iron beads, *European Physical Journal B* **18**, 337-341 (2000)

[14] F.J. Lowes and I. Wilkinson, *Nature* **198**, 1158-1160 (1963), *Nature* **219**, 717-718 (1968)

[15] E. N. Parker, *Astrophys. J.* **122**, 293 (1955)

[16] M. Steenbeck et al., *Sov. Phys. Dokl.* **13**, 443 (1968).

[17] F. Pétrélis, M. Bourgoin, L. Marié, A. Chiffaudel, S. Fauve, F. Daviaud, P. Odier and J.-F. Pinton: Non linear induction in a swirling flow of liquid sodium, *Phys. Rev. Lett.*, **90**(17), 174501, (2003)

[18] M. Bourgoin, R. Volk, P. Frick, S. Kripechenko, P. Odier, J.-F. Pinton, Induction mechanisms in von Kármán swirling flows of liquid Gallium, *Magnetohydrodynamics*, **40**(1), 13-31, (2004)

[19] C. Simand, F. Chillà, J.-F. Pinton : Study of inhomogeneous turbulence in the closed flow between corotating disks, *Europhysics Letters* **49**, 336 (2000)

[20] N.O. Weiss, *Proc. R. Soc. London, Ser. A***293**, 310 (1966)

[21] P. Odier, J.-F. Pinton, and S. Fauve, *Eur. Phys. J. B* **16**, 373 (2000)

[22] F. Stefani, M. Xu, G. Gerbeth, F. Ravelet, A. Chiffaudel, F. Daviaud and J. Lorat, Ambivalent effects of added layers on steady kinematic dynamos in cylindrical geometry: application to the VKS experiment, *Eur. J. Mech. B-Fluids* **25**(6), 894 (2006)

[23] Xu M, Stefani F, Gerbeth G, *J. Comp. Phys.* **227**(17), 8130 (2008)

[24] Avalos-Zuniga R, Plunian F, Influence of inner and outer walls electromagnetic properties on the onset of a stationary dynamo, **Euro. Phys. J. B 47**(1), 127 (2005)

[25] Gissinger C, Iskakov A, Fauve S, Dormy E, Effect of magnetic boundary conditions on the dynamo threshold of von Karman swirling flows, *Europhys. Lett.* **82**(2), 29001 (2008)

[26] DH Kelley DH , SA Triana SA, DS Zimmerman DS, A. Tilgner A , DP Lathrop DP, Inertial waves driven by differential rotation in a planetary geometry, *GAFD* **101**(5-6), 469-487 (2007)

[27] D. Schmitt, T. Alboussiere, D. Brito, P. Cardin, N. Gagniere, D. Jault, HC Nataf, Rotating spherical Couette flow in a dipolar magnetic field: experimental study of magneto-inertial waves, *J. Fluid Mech.* **604**, 175-197 (2008)

[28] R. Volk, R. Monchaux, M. Berhanu, F. Ravelet, A. Chiffaudel, F. Daviaud, B. Dubrulle, S. Fauve, N. Mordant, Ph. Odier, F. Pétrélis and J.-F. Pinton, Transport of magnetic field by a turbulent flow of liquid sodium, *Phys. Rev. Lett.* **97** 074501 (2006)

[29] F. Ravelet, R. Volk, A. Chiffaudel, F. Daviaud, B. Dubrulle, R. Monchaux, M. Bourgoin, P.

Odier, J.-F. Pinton, M. Berhanu, S. Fauve, N. Mordant, F. Petrelis, Magnetic induction in a turbulent flow of liquid sodium: mean behaviour and slow fluctuations, `arXiv:0704.2565`

[30] N.L. Peffley, A. B. Cawthorne, and D.P. Lathrop, Toward a self-generating magnetic dynamo: The role of turbulence, *Phys. Rev. E* **61**(5), 5287 (2000)

[31] F. Krause and K.-H. Rädler, *Mean field magnetohydrodynamics and dynamo theory*, Pergamon Press (New-York, 1980).

[32] KH Radler, R Stepanov, Mean electromotive force due to turbulence of a conducting fluid in the presence of mean flow, *Phys. Rev. E* **73**(5), 056311 (2006)

[33] M. Dikpati and P.A. Gilman, Flux-Transport Dynamos with α-Effect from Global Instability of Tachocline Differential Rotation: A Solution for Magnetic Parity Selection in the Sun, *Astrophys. J* **559**(1), 428-442 (2001)

[34] G.O. Roberts, *Philos. Trans. R. Soc. London*, **A271**, 411454 (1972)

[35] Busse, F. H. Dynamo theory of planetary magnetism and laboratory experiments. In Evolution of Dynamical Structures in Complex Systems (ed. R. Friedrich and A. Wunderlin), pp. 359384. Springer (1992)

[36] Tilgner, A. 1997 A kinematic dynamo with a small scale velocity field. Phys. Lett. A 226, 7579.

[37] Tilgner, A. 2002 Numerical simulation of the onset of dynamo action in an experimental two-scale dynamo. Phys. Fluids 14, 40924094.

[38] Tilgner, A. Busse, F. H. 2002 Simulation of the bifurcation diagram of the Karlsruhe dynamo. Magnetohydrodynamics 38, 3540.

[39] Frick P., Noskov V., Denisov S., Khripchenko S., Sokoloff D., Stepanov R., and Sukhanovsky A. Non-stationary screw flow in a toroidal channel: way to a laboratory dynamo experiment. *Magnetohydrodynamics*, 2002. V.38. N.1-2. P.136-155.

[40] Denisov S., Noskov V., Sukhanovskiy A., and Frick P. Unsteady turbulent spiral flows in a circular channel. *Fluid Dynamics*, **36**(5), pp734-742 (2001)

[41] Chen QN, Chen SY, Eyink GL, The joint cascade of energy and helicity in three-dimensional turbulence, *Phys. Fluids* **15**(2), 361-374 (2003)

[42] R. Stepanov, R. Volk, S. Denisov, P. Frick, V. Noskov, J.-F. Pinton, Induction, helicity and alpha effect in a toroidal screw flow of liquid gallium, *Phys. Rev. E* **73**, 046310 (2006)

[43] A. B. Reighard and M. R. Brown, Turbulent Conductivity Measurements in a Spherical Liquid

Sodium Flow, *Phys. Rev. Lett.* **86**(13), 2794 (2001)

[44] S. A. Denisov, V. I. Noskov, R. A. Stepanov, and P. G. Frick, Measurements of Turbulent Magnetic Diffusivity in a Liquid-Gallium Flow, *JETP Letters* **88**(3), 167-171 (2008)

[45] M. Bourgoin, P. Odier, J.-F. Pinton and Y. Ricard, An iterative study of time independent induction effects in magnetohydrodynamics, *Phys. Fluids*, **16**(7), 2529–2547, (2004)

[46] Spence et al. Observation of a turbulence–induced large scale magnetic field, *Phys. Rev. Lett.* **96**, 055002 (2006)

[47] T. G. Cowling, *Mon. Not. R. Astron. Soc.* **94**, 39 (1934)

[48] E. C. Bullard, The stability of a homopolar dynamo, *Proc. Camb. Phil. Soc* **51**, 744 (1955)

[49] D. Sweet, E. Ott, J. M. Finn, T. M. Antonsen Jr., D. P. Lathrop, Blowout bifurcations and the onset of magnetic activity in turbulent dynamos, *Phys. Rev. E* **63**, 066211 (2001)

D. Sweet, E. Ott, T.M. Antonsen TM, D.P. Lathrop, Blowout bifurcations and the onset of magnetic dynamo action, *Phys. Plasmas* **8**, 1944-1952 (2001)

[50] M. Bourgoin, R. Volk, N. Plihon, P. Augier, Ph. Odier, J.-F. Pinton: A Bullard von Kármán dynamo, *New J. Phys.* **8**, 329, (2006)

[51] G. Verhille, N. Plihon, R. Volk, M. Bourgoin, P. Odier and J.-F. Pinton,Large scale fluctuations and dynamics of the Bullard - von Kármán dynamo, `arXiv`

[52] S. Aumaitre, F. Pétrélis and K. Mallick, Low frequency noise controls on-off intermittency of bifurcating systems, *Phys. Rev. Lett.* **95**, 064101 (2005)

S. Aumaitre, K. Mallick and F. Pétrélis, Effects of the low frequencies of noise on on-off-bifurcations, *J. Stat. Phys.* **123**, 909 (2006)

S. Aumaitre and F. Pétrélis, Modification of instability processes by multiplicative noises, *Eur. J. Phys.* **B51**, 357 (2006)

[53] Yu.B.Ponomarenko, *J. Appl. Mech. Tech. Phys.***14**, 775779 (1973)

[54] A. Gailitis and Ya. Freibergs, *Magnetohydrodynamics* **12**, 127129 (1976)

[55] A. Gailitis, *Magnetohydrodynamics***32**, 5862 (1996)

[56] A. Gailitis et al., *Phys. Rev. Lett.* **86**, 30243027 (2001)

A. Gailitis, O. Lielausis, E. Platacis, G. Gerbeth, F. Stefani, *Magnetohydrodynamics***38**, 15-26 (2002)

A. Gailitis, O. Lielausis, E. Platacis, G. Gerbeth, and F. Stefani, *Rev. Mod. Phys.***74**, 973-990 (2002)

[57] A. Tilgner, F. Busse, *Magnetohydrodynamics* **38**, 35-40 (2002). K.-H. Rädler, M. Rheinhardt, E. Apstein, *Magnetohydrodynamics* **38**, 41-71 (2002).

[58] Müller U, Stieglitz R, Horanyi S, Experiments at a two-scale dynamo test facility, *J. Fluid Mech.* **552**, 419 (2006).

U. Müller, R. Steiglitz, F. H. Busse, A. Tilgner, *C.R. Physique* **9**, 729-740 (2008)

[59] R. Monchaux, M. Berhanu, M. Bourgoin, M. Moulin, Ph. Odier, J.-F. Pinton, R. Volk, S. Fauve, N. Mordant, F. Pétrélis, A. Chiffaudel, F. Daviaud, B. Dubrulle, C. Gasquet, L. Marié, F. Ravelet, Generation of magnetic field by dynamo action in a turbulent flow of liquid sodium, *Phys. Rev. Lett.* **98** 044502, (2007)

[60] M. Berhanu, R. Monchaux, M. Bourgoin, M. Moulin, Ph. Odier, J.-F. Pinton, R. Volk, S. Fauve, N. Mordant, F. Pétrélis, A. Chiffaudel, F. Daviaud, B. Dubrulle, C. Gasquet, L. Marié, F. Ravelet, Magnetic field reversals in an experimental turbulent dynamo, *Europhys. Lett.* **77**, 59007 (2007)

[61] Monchaux R, Ravelet F, Dubrulle B, Daviaud F, Properties of steady states in turbulent axisymmetric flows, *Phys. Rev. Lett.***96**(12), 124502 (2006)

Ravelet F, Chiffaudel A, Daviaud F, Supercritical transition to turbulence in an inertially driven von Karman closed flow, *J. Fluid Mech.* **601**, 339 (2008)

[62] S. Aumaître, M. Berhanu, M. Bourgoin, A. Chiffaudel, F. Daviaud, B. Dubrulle, S. Fauve, L. Marié, R. Monchaux, N. Mordant, Ph. Odier, F. Pétrélis, J.-F. Pinton, N. Plihon, F. Ravelet, R. Volk, The VKS experiment: turbulent dynamical dynamos, *Comptes Rendus de l'Académie des Sciences* **9**(7), 689 (2008)

[63] R. Monchaux, M. Berhanu, S. Aumaître, A. Chiffaudel, F. Daviaud, B. Dubrulle, F. Ravelet, M. Bourgoin, Ph. Odier, J.-F. Pinton, N. Plihon, R. Volk, S. Fauve, N. Mordant, F. Pétrélis, Chaotic dynamos generated by a turbulent flow of liquid sodium, *Phys. Rev. Lett.* **101**, 074502 (2008)

[64] R. Monchaux, M. Berhanu, S. Aumaître, A. Chiffaudel, F. Daviaud, B. Dubrulle, L. Marié, F. Ravelet, S. Fauve, N. Mordant, F. Pétrélis, M. Bourgoin, P. Odier, J.-F. Pinton, N. Plihon, R. Volk, The VKS experiment: turbulent dynamical dynamos, to appear in *Phys. Fluids* (2009)

[65] L. Marié, J. Burguete, F. Daviaud and J. Léorat, Numerical study of homogeneous dynamo based on experimental von Kármán type flows, *Eur. Phys. J. B* **33**, 469-485 (2003)

[66] F. Ravelet, A. Chiffaudel, F. Daviaud and J. Léorat, Toward an experimental von Kármán

dynamo: Numerical studies for an optimized design, *Phys. Fluids* **17**, 117104 (2005)

[67] M. Bourgoin, L. Marié, F. Pétrélis, C. Gasquet, A. Guigon, J.-B. Luciani, M. Moulin, F. Namer, J. Burguete, A. Chiffaudel, F. Daviaud, S. Fauve, Ph. Odier, and J.-F. Pinton, Magnetohydrodynamics measurements in the von Kármán sodium experiment, *Phys. Fluids* **14**, 3046-3058 (2002)

[68] R. Volk, R. Monchaux, M. Berhanu, F. Ravelet, A. Chiffaudel, F. Daviaud, B. Dubrulle, S. Fauve, N. Mordant, Ph. Odier, F. Pétrélis and J.-F. Pinton, Transport of magnetic field by a turbulent flow of liquid sodium, *Phys. Rev. Lett.* **97** 074501 (2006)

[69] F. Pétrélis and S. Fauve, Saturation of the magnetic field above the dynamo threshold, *Eur. Phys. J. B* **22**, 273-276 (2001)

[70] L. Marié, Transport de moment cinétique et de champ magnétique par un écoulement tourbillonnaire turbulent: influence de la rotation, *PhD thesis, Université de Paris 7* (2003), `http://tel.archives-ouvertes.fr/tel-00007755/en/`

[71] R. Monchaux, Mécanique statistique et effet dynamo dans un écoulement de von Kármán turbulent, *PhD thesis Université Diderot, Paris 7* (2007), `http://tel.archives-ouvertes.fr/tel-00199751/en/`

[72] Biblio Morin, Christensen ... sur la proximit de modes dipole et quadrupole.

[73] Ph. Nozières, Reversals of the Earths magnetic field: an attempt at a relaxation model. *Physics of the Earth and Planetary Interior***17**, 5574 (1978)

[74] F. Pétrélis and S. Fauve, Chaotic dynamics of the magnetic field generated by dynamo action in a turbulent flow, *J. Phys.: Condens. Matter* **20** 494203 (2008)

[75] Sisan et al., Experimental Observation and Characterization of the Magnetorotational Instability, *Phys. Rev. Lett.* **93**(11), 114502 (2004)

[76] D. Schmitt et al. Rotating spherical Couette flow in a dipolar magnetic field: experimental study of magneto-inertial waves, *Journal of Fluid Mechanics* **604**, 175 (2008)

[77] G. Verhille, N. Plihon, J.-F. Pinton, V. Noskov, R. Stepanov, P. Frick, Velocity measurement in a spin-down flow inside a torus, submitted to *Phys. Fluids* (11/2008)

[78] Odier et al. *Phys. Rev. E* **58**(6) (1998)

[79] H.F. Beckley, Measurement of annular Couette flow stability at the fluid Reynolds number $Re = 4.4\ 10^6$: the fluid dynamic precursor to a liquid sodium $\alpha\omega$ dynamo, PhD Dissertation, New Mexico Institute of Mining and Technology (2002)

[80] E.P. Velikhov, Phys. Lett. A. 358, 216-221 (2006).

[81] G. Rüdiger et al., Astrophys. J. 649, L145-L147 (2006).

F. Stefani et al., Phys. Rev. Lett. 97, 184502 (2006).

F. Stefani et al., New J. Phys. 9, 295 (2007).